Measurement 149 (2020) 107036

Contents lists available at ScienceDirect

Measurement

journal homepage: www.elsevier.com/locate/measurement

Fault diagnosis of rolling bearings using weighted horizontal visibility graph and graph Fourier transform

Yiyuan Gao, Dejie Yu *, Haojiang Wang

State Key Laboratory of Advanced Design and Manufacturing for Vehicle Body, Hunan University, Changsha 410082, China

ARTICLE INFO

Article history:
Received 13 April 2019
Received in revised form 23 August 2019
Accepted 4 September 2019
Available online 7 September 2019

Keywords:
Fault diagnosis
Rolling bearing
Weighted horizontal visibility graph
Graph Fourier transform
Fault impulse component

ABSTRACT

Graph Fourier transform (GFT) has been proven to be an effective tool for impulse component extraction of rolling bearings, but its performance is closely related to the structure of underlying graph. Compared with the weighted path graph, the weighted horizontal visibility graph (WHVG) can reflect the dynamics characteristics of vibration signals better. When the fault bearing vibration signal is transformed into the WHVG, GFT can cluster most of the fault impulse component to the highest order range and has strong anti-interference ability. Based on WHVG and GFT, a novel fault diagnosis method for rolling bearings is proposed. In the proposed method, the graph spectrum coefficients in the highest order range are extracted to reconstruct the fault impulse component, and then the Hilbert envelope spectrum is used to diagnose the bearing fault. Simulation and experimental results demonstrate that the proposed fault diagnosis method for rolling bearings is noise tolerant and effective.

1. Introduction

Rolling bearings are the key components of rotating machines, so the faulty rolling bearings can directly affect the working performance and operating life of mechanical equipment. It is well known that the rolling bearing fault is one of the most common causes of mechanical failures in practical engineering applications, and the consequences may range from breakdown maintenance to catastrophic accident [1,2]. Hence, it is very meaningful to inspect the bearing health at regular intervals. In general, vibration signal analysis is one of the preferred methods for fault diagnosis of rolling bearings. However, due to the harsh working conditions, the collected vibration signal contains not only the fault impulse component but also the strong interference components, such as harmonic component and strong background noise [3,4]. Accordingly, extracting the fault impulse component from vibration signals is the key to fault diagnosis of rolling bearings.

For effectively extracting the fault impulse component from original vibration signals, many signal processing methods, such as the time-domain averaging, wavelet transform, empirical wavelet transform, band-pass filtering, matching pursuit, empirical mode decomposition, ensemble empirical mode decomposition and so on, have been proposed and applied to the fault diagnosis of rolling bearings [5–14]. Although a great number of positive results have been achieved, there are still some shortcomings in these existing methods. For example, the selections of mother wavelet and decomposition layer are not adaptive in wavelet transform [6]; empirical mode decomposition has the problems of mode mixing, end effects, over envelope and under envelope in the process of adaptive decomposition [10]. Among these existing methods, the band-pass filtering method usually combined with a demodulation technique was early developed and still widely used, but how to properly select the central frequency and bandwidth in this method is a major challenge. To solve this problem, the spectral kurtosis method [15] was proposed, which has been proven to be very useful for detecting the fault impulse component. Its basic idea is to treat the kurtosis as an indicator to detect the existence of fault impulse component and to point out the optimal frequency band in which the fault impulse component appears. However, the spectral kurtosis method is usually applied on the basis of the short-time Fourier transform (STFT) and finite impulse response (FIR) filters, both of which also have inherent defects [16]. For example, the STFT cannot consider time resolution and frequency resolution simultaneously due to the limitation of fixed window length, and the FIR filters are unlikely to achieve the best match with each fault characteristic signal.

Abbreviations: FT, Fourier transform; GFT, graph Fourier transform; IGFT, inverse graph Fourier transform; WPG, weighted path graph; WHVG, weighted horizontal visibility graph; STFT, short-time Fourier transform; FIR, finite impulse response; SNR, signal-to-noise ratio.

* Corresponding author.
E-mail address: djyu@hnu.edu.cn (D. Yu).

https://doi.org/10.1016/j.measurement.2019.107036
0263-2241/

Therefore, it is necessary to further explore the new extraction method of fault impulse component for rolling bearings.

In recent years, a new research field, namely graph signal processing [17], has emerged with the development of spectral graph theory and algebraic signal processing theory. Its basic idea is to extend the conventional signal processing concepts and techniques to the signals indexed by general graphs, i.e. graph signals. Aliaksei Sandryhaila et al. [18,19] proposed the techniques of discrete signal processing on graph, which includes the notions of shift, filtering, convolution, Fourier transform, spectral decomposition and impulse response defined on graph signals. In order to realize the "vertex-frequency" analysis of graph signals, David I Shuman et al. [20] defined the concepts of translation operator and modulation operator for graph signals, and used these two operators to design the windowed graph Fourier transform. In addition, other graph signal processing techniques, for example, graph wavelet transform [21,22], graph empirical mode decomposition [23] and graph Hilbert transform [24], have also been proposed. Different from the traditional signal processing methods, these graph signal processing techniques analyze the graph structure that represents the internal relationships of the dataset rather than the dataset itself. Therefore, they can extract the feature information hidden in a very large dataset more effectively, and have been successfully applied to sensor networks, image processing, bridge health monitoring and other fields [17,25,26].

As is well known, the basis of the traditional signal processing methods is the Fourier transform (FT). Similarly, the basis of the graph signal processing techniques is the graph Fourier transform (GFT). The GFT [17,18] is defined as the expansion of graph signals based on the eigenvectors of the graph Laplacian matrix or the graph adjacency matrix, and can transform the graph signals from the vertex domain to the graph spectrum domain. As far as mechanical fault diagnosis is concerned, the role of the FT cannot be ignored. Similarly, GFT can also play an important role in mechanical fault diagnosis. In order to introduce the GFT into the field of mechanical fault diagnosis, it is necessary to transform mechanical vibration signals into suitable graph signals. For this purpose, Lu Ou et al. [27–29] have regarded mechanical vibration signals as path graph signals in a manifold perspective. However, path graph is the simplest and most intuitive graph structure, and the same structure of path graphs will be obtained for different mechanical vibration signals with the same sampling points. Thus, the path graph cannot fully reflect the dynamics characteristics of a mechanical vibration signal. From this point of view, a more suitable graph structure should be found for mechanical vibration signals to improve the ability of GFT in mechanical fault diagnosis. In order to characterize time series more effectively with complex network theory, Luque et al. [30] proposed the horizontal visibility algorithm in 2009. This algorithm can exactly map the dynamics characteristics of a random time series into the topological properties of a horizontal visibility graph. Since the mechanical vibration signal is a typical time series, it can also be transformed into a horizontal visibility graph by means of the horizontal visibility algorithm.

Impulses and harmonics are the two main components of the fault bearing vibration signals. Lu Ou et al. [27,28] found that the GFT combined with weighted path graph has obvious clustering characteristic. That is to say, the GFT can cluster the impulse and harmonic components to different order ranges of graph spectrum. The key role of the clustering characteristics of the GFT is the graph Laplacian eigenvectors that are the basis functions of the GFT. When the vibration signal of faulty bearing is transformed into the weighted path graph (WPG), the GFT can cluster most of the fault impulse components to the highest order range of graph spectrum. Based on this point, Lu Ou et al. [27] proposed a new impulse component extraction method for rolling bearings, which is referred to as the WPG-GFT method for simplicity in this study. We found that when the vibration signal of faulty bearing is transformed into the weighed horizontal visibility graph (WHVG), the GFT can also cluster more of the fault impulse components to the highest order range of graph spectrum. The advantage is that the WHVG based GFT has stronger anti-interference ability than the WPG based GFT in clustering characteristic. Thus, based on WHVG and GFT, we propose a novel impulse component extraction method for better diagnosing the rolling bearing faults, which is referred to as the WHVG-GFT method for simplicity in this study. In the WHVG-GFT method, the vibration signal collected from a faulty rolling bearing is first transformed into a WHVG by means of the horizontal visibility algorithm, and then the vibration signal is indexed by its WHVG to acquire the vibration graph signal. Next, the vibration graph signal is subjected to the GFT to obtain the graph spectrum. Since most of the fault impulse components are clustered to the highest order range of graph spectrum, the inverse graph Fourier transform (IGFT) is carried out to extract the fault impulse component in the vibration signal after retaining the last few graph spectrum coefficients and discarding the remaining coefficients. Finally, the rolling bearing fault can be identified by the Hilbert envelope spectrum of the extracted fault impulse component. Simulation and experimental results demonstrate that the WHVG-GFT method is superior to the WPG-GFT and spectral kurtosis methods in the diagnosis of outer and inner ring faults of rolling bearings.

To sum up, this paper is an improved version of the literature [27]. In the literature [27], the GFT is combined with the WPG to extract the fault impulse component of rolling bearings. In this paper, the GFT is combined with the WHVG to extract the fault impulse component of rolling bearings. Therefore, the innovation of this paper lies in the introduction of WHVG to vibration signal analysis, which can greatly improve the performance of GFT in rolling bearing fault diagnosis. The remaining parts of this paper are arranged as follows. The definitions of the WHVG and GFT are given in Section 2. The WHVG based GFT analysis of the impulse and harmonic components is introduced in Section 3. A novel rolling bearing fault diagnosis method using WHVG and GFT is presented in Section 4. The simulation analysis and experimental validations of the WHVG-GFT method are respectively performed in Sections 5 and 6. Finally, the conclusions of this study are provided in Section 7.

2. Weighted horizontal visibility graph and graph Fourier transform

2.1. Weighted horizontal visibility graph

The core of graph signal processing techniques is to analyze the signals indexed by representation graphs. Generally, the representation graphs consist of a finite number of vertices and edges connecting the vertices. In 2009, the horizontal visibility algorithm [30] was proposed, which can exactly map the dynamics characteristics of a random time series into the topological properties of a horizontal visibility graph. The definition of the horizontal visibility algorithm is described below. Let $\{x(i)\}_{i=1,\cdots,N}$ be a time series with N values that can be any real number, the horizontal visibility algorithm will assign each value of the time series to each vertex of the horizontal visibility graph in sequence, so the time series with N values can be mapped to a horizontal visibility graph with N vertices. If the following geometric standard is satisfied in the time series, vertices v_i and v_j in the horizontal visibility graph will be connected by an undirected edge.

$$x(i), x(j) > x(n), \quad \forall n \mid i < n < j. \tag{1}$$

where $x(i)$ and $x(j)$ can be any two different values of the time series, and $x(n)$ are all the values between them.

An illustrative example is given in Fig. 1. Firstly, the data heights (values) of a time series {0.9 0.5 0.4 0.8 0.9 0.5 0.4 0.8 0.9 0.5 0.4 0.8} is plotted in Fig. 1(a) by using vertical bars. Then, in Fig. 1(a), we connect every bar (every value of the time series) with all those that can be seen horizontally from any position of the considered one. In other words, two bars are connected by a horizontal visibility line if their heights are greater than the heights of all the bars between them. Finally, the horizontal visibility graph shown in Fig. 1(b) can be obtained, whose vertices and edges respectively correspond to the bars and horizontal visibility lines in Fig. 1(a) in sequence.

Since the rolling bearing vibration signal is a typical time series, it can also be mapped into a horizontal visibility graph through the horizontal visibility algorithm. In general, a weighted horizontal visibility graph (WHVG) can be symbolized as $G = \{V, E, \mathbf{W}\}$, where $V = \{v_1, \cdots, v_N\}$ represents a finite set of vertices, E represents a set of edges connecting the vertices, and $\mathbf{W}$ is the weighted graph adjacency matrix. The element of $\mathbf{W}$ at the ith row and jth column is denoted as w_{ij}, and if vertex v_i and vertex v_j are connected by one undirected edge, $w_{ij} = w_{ji}$ representing the weight of the edge is nonzero, otherwise, $w_{ij} = w_{ji} = 0$. In order to remove the self-loop of vertices, w_{ii} is set as 0. For the sake of better reflecting the difference between vertices, the nonzero w_{ij} in this study is defined as

$$w_{ij} = \| x(i) - x(j) \|^2 \tag{2}$$

where $x(i)$ and $x(j)$ are the signal values indexed by vertex v_i and vertex v_j, respectively. The graph Laplacian matrix $\mathbf{L}$ is calculated by the graph adjacency matrix $\mathbf{W}$ and degree diagonal matrix $\mathbf{D}$ whose ith diagonal element $d_i = \sum_{j \neq i} w_{ij}$, and its definition is shown in Eq. (3).

$$\mathbf{L} = \mathbf{D} - \mathbf{W} \tag{3}$$

The graph Laplacian matrix can reflect the topological properties of a graph structure more comprehensively than the graph adjacency matrix and degree diagonal matrix because it not only contains the connection information between vertices, but also contains the degree information of vertices. In reality, the graph Laplacian matrix is a real symmetric matrix, so it has a set of real and non-negative eigenvalues $\{\lambda_l\}_{l=0,1,\cdots,N-1}$ and a complete set of orthonormal eigenvectors $\{\mathrm{u}_l\}_{l=0,1,\cdots,N-1}$. These eigenvalues and eigenvectors satisfy

$$\mathbf{L}\mathrm{u}_l = \lambda_l \mathrm{u}_l \tag{4}$$

2.2. Graph Fourier transform

In this study, vibration signals indexed by the corresponding horizontal visibility graphs are referred to as the vibration graph signals X, and the vibration graph signals X can be defined as a mapping from a set of vertices V to a set of real numbers $\mathbb{R}$:

$$\begin{aligned} &\mathrm{X} : \mathrm{V} \rightarrow \mathbb{R}, \\ &v_i \mapsto x(i). \end{aligned} \tag{5}$$

The mapping (5) can also be written as

$$\mathrm{X} = [x(1), x(2), \cdots, x(N)]^T \in \mathbb{R}^N,$$

where the value $x(i)$ of vibration signals is indexed by the vertex v_i of their horizontal visibility graph. The space S of the vibration graph signals X is isomorphic to $\mathbb{R}^N$, and the dimension of the vibration graph signals X is dim $S = N$.

With the horizontal visibility algorithm as a bridge, the GFT can be introduced to analyze the vibration signals. It is well known that the FT is defined as the expansion of regular signals based on the eigenfunctions of the one-dimensional Laplace operator. Similarly, the definition of GFT [17,18] is the expansion of graph signals based on the eigenvectors of the graph Laplacian matrix or adjacency matrix. In this study, the GFT is defined by the graph Laplacian matrix, as shown in Eq. (6), and the IGFT is also given as shown in Eq. (7) [17].

$$\hat{x}(l) = \sum_{i=1}^{N} x(i) u_l(i), \ l = 0, 1, \cdots, N-1 \tag{6}$$

$$x(i) = \sum_{l=0}^{N-1} \hat{x}(l) u_l(i), \ i = 1, 2, \cdots, N \tag{7}$$

where $\hat{x}(l)$ is the graph spectrum coefficients, $x(i)$ is the value of vibration graph signals X, and $u_l(i)$ is the value of the corresponding eigenvectors of graph Laplacian matrix.

The GFT and IGFT provide a very good way to equivalently represent the graph signals in two different domains. In other words, the GFT is able to convert the graph signals from the vertex domain to the graph spectrum domain, and the IGFT is able to convert the graph signals from the graph spectrum domain to the vertex domain.

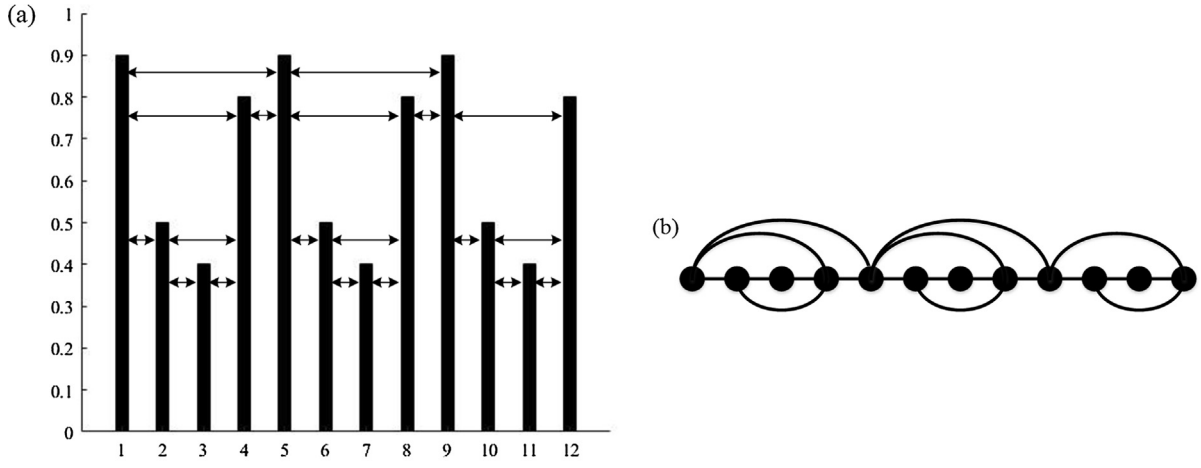

Fig. 1. Data heights (values) and horizontal visibility graph of the time series. (a) Data heights (values); (b) Horizontal visibility graph.

3. The WHVG based GFT analysis of the impulse and harmonic components

Spectral clustering [31] has been widely studied and applied because of its simple implementation and good clustering effect. The graph Laplacian eigenvectors play a key role in spectral clustering because they contain the clustering information of the original sample data. For the sake of making the GFT have clustering characteristic, in other words, the ability of clustering signals with the same features together, the eigenvectors of the graph Laplacian matrix rather than adjacency matrix are selected as the basis functions of GFT in this study. Based on the clustering characteristic of GFT, we believe that the impulse and harmonic components in a fault bearing vibration signal can be effectively separated. To test and verify this idea, the simulated impulse and harmonic components are first considered. When the rolling bearing has a localized fault, the simulated impulse component $h(t)$ can be expressed as follows [32]

$$h(t) = \sum_{m=0}^{M-1} B_m \exp[-\beta(t - mT)] \times \cos[2\pi f_{re} \times (t - mT)] u(t - mT) \tag{8}$$

where B_m is the amplitude of the mth impulse, β is the structural damping ratio, T is the impulse interval, f_{re} is the resonance frequency, and $u(t)$ is the unit step function. The sampling frequency and sampling time of the simulated impulse component are taken as 4096 Hz and 0.5 s, respectively, and the fault characteristic frequency f_c is equal to $1/T$, that is, 50 Hz. The simulated impulse component can be obtained by substituting the values of the corresponding parameters shown in Table 1 into Eq. (8), and its time domain waveform is plotted in Fig. 2(a).

As shown in Eq. (9), the simulated harmonic component $s(t)$ superimposed by two sinusoidal signals, is considered in this study. The sampling frequency and sampling time of the simulated harmonic component are the same as those of the simulated impulse component. The simulated harmonic component can be obtained by substituting the values of the frequencies f_1 and f_2 shown in Table 1 into Eq. (9), and its time domain waveform is drawn in Fig. 2(b).

$$s(t) = 1.2\sin(2\pi f_1 t) + 1.2\sin(2\pi f_2 t) \tag{9}$$

The simulated impulse and harmonic components can be transformed into two different horizontal visibility graphs by Eq. (1), and the weight of their edges is defined by Eq. (2), namely the WHVG1 and WHVG2, respectively. Here, the simulated impulse component indexed by the WHVG1 is known as the impulse graph signal whose values correspond to the values of the simulated impulse component one by one, and the simulated harmonic component indexed by the WHVG2 is called the harmonic graph signal whose values correspond to the values of the simulated harmonic component one by one. Ultimately, their frequency spectra shown in Fig. 3 can be obtained by performing the FT on the simulated impulse and harmonic components, and their graph spectra displayed in Fig. 4 can be gained by performing the GFT on the impulse and harmonic graph signals.

As can be observed from Fig. 3, the simulated impulse and harmonic components in the frequency spectra cannot be separated because the FT has no clustering characteristic. Surprisingly, we can see from Fig. 4 that the energy of the simulated impulse component is largely distributed in highest order range, while that of the simulated harmonic component is largely distributed in the lower order range. This indicates that the GFT has obvious clustering characteristic, and the simulated impulse and harmonic components can be effectively separated by the GFT. Thus, we can reconstruct the fault impulse component in the rolling bearing vibration signal by only retaining the last few graph spectrum coefficients and discarding the remaining coefficients. Using this

Table 1
Parameters of the simulated impulse and harmonic components.

M	B_m	β	f_{re}	T	f_1	f_2
24	3	1200	420	1/50	200	400

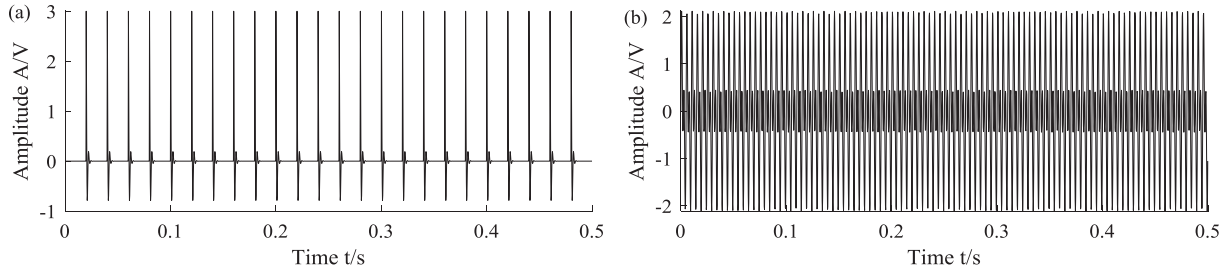

Fig. 2. Time domain waveforms of the simulated impulse and harmonic components. (a) Simulated impulse component; (b) Simulated harmonic component.

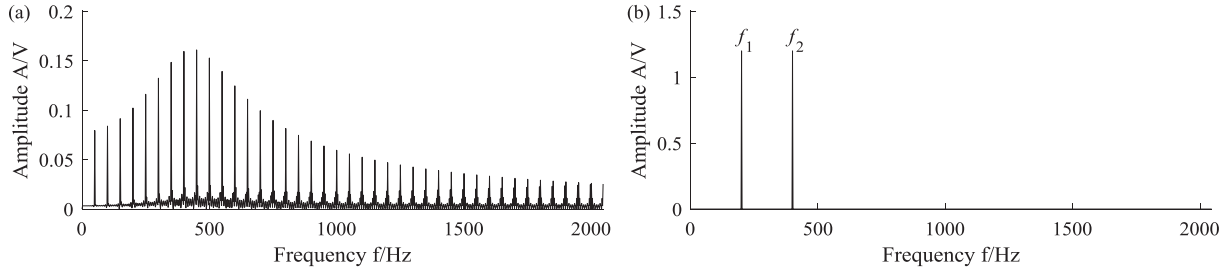

Fig. 3. Frequency spectra of the simulated impulse and harmonic components. (a) Simulated impulse component; (b) Simulated harmonic component.

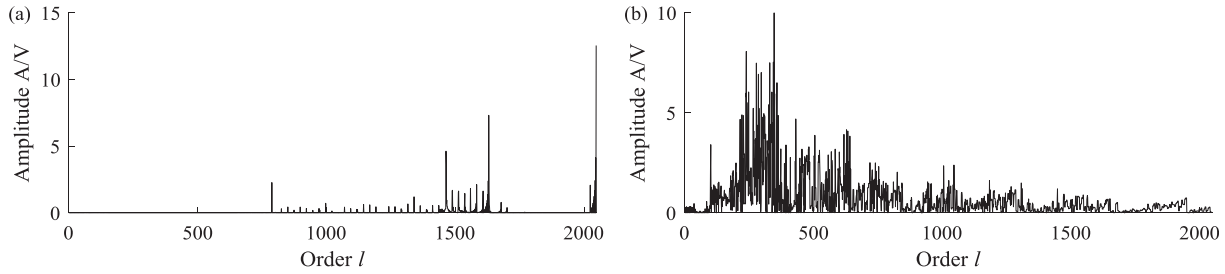

Fig. 4. Graph spectra of the simulated impulse and harmonic components. (a) Simulated impulse component; (b) Simulated harmonic component.

property, it is feasible to extract the fault impulse component from the rolling bearing vibration signal to diagnose the rolling bearing fault.

4. Rolling bearing fault diagnosis using WHVG and GFT

The periodic impulses contained in the vibration signal are important indicators of rolling bearing failure. Nevertheless, the fault-caused impulse component is usually too weak to be easily recognized because of many interference components, especially the harmonic component and strong background noise. Therefore, extracting the fault impulse component from its vibration signal is very significant for the fault diagnosis of rolling bearings. For better extracting the fault impulse component, the WHVG and GFT are simultaneously introduced to analyze the rolling bearing vibration signals. It has been found that the GFT has obvious clustering characteristic. After transforming the simulated impulse and harmonic components into the WHVG, the GFT can cluster them to different order ranges, and the simulated impulse component is largely clustered to the highest order range. In this study, taking advantage of this clustering characteristic of GFT, the WHVG-GFT method is presented for rolling bearing fault diagnosis. The detailed steps of the WHVG-GFT method are as following:

(1) Transform the vibration signal collected from a faulty rolling bearing into a horizontal visibility graph according to Eq. (1).
(2) Weight the edges of the horizontal visibility graph according to Eq. (2) to obtain the WHVG.
(3) Define the vibration signal on the WHVG according to Eq. (5) to acquire the vibration graph signal.
(4) Perform the GFT on the vibration graph signal according to Eq. (6) to obtain the graph spectrum.
(5) Carry out the IGFT after retaining the last graph spectrum coefficients and discarding the remaining coefficients according to Eq. (7) to extract the fault impulse component in the vibration signal.
(6) Identify the rolling bearing fault through the Hilbert envelope spectrum of the extracted fault impulse component.

The flow chart of the WHVG-GFT method is displayed in Fig. 5.

5. Simulation analysis

Generally, when a localized fault is induced in the inner ring or outer ring of rolling bearings, periodic impulses whose repetition frequency is the fault characteristic frequency will appear in their vibration signals. For validating the effectiveness of the WHVG-GFT method in extracting the fault impulse component, a synthetic signal $z(t)$ is established by Eq. (10) to simulate the fault bearing vibration signal.

$$z(t) = h(t) + s(t) + n(t) \tag{10}$$

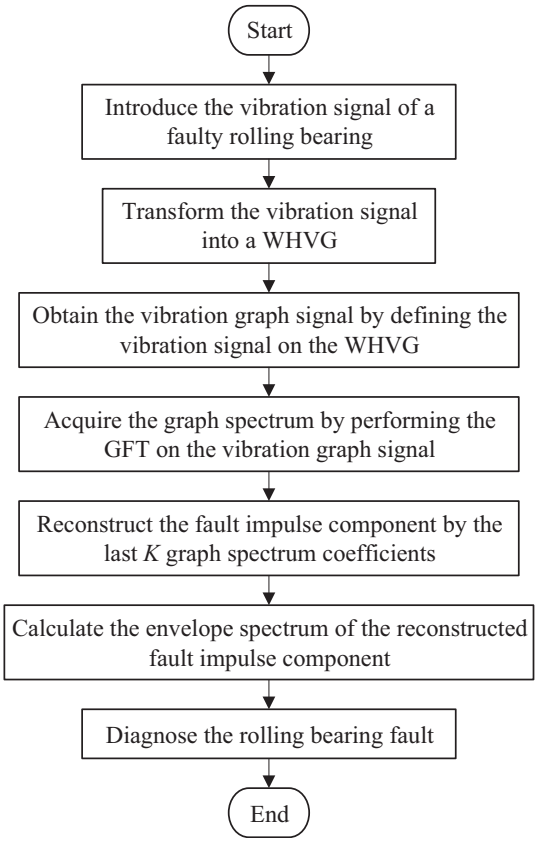

Fig. 5. Flow chart of the WHVG-GFT method.

where $h(t)$ is the simulated impulse component shown in Eq. (8), $s(t)$ is the simulated harmonic component shown in Eq. (9), and $n(t)$ is the Gaussian white noise. In the beginning, the signal-to-noise ratio (SNR) of the synthetic signal $z(t)$ is set as −1dB.

The sampling frequency and sampling time are set respectively as 4096 Hz and 0.5 s, and the fault characteristic frequency f_c is equal to 50 Hz. The synthetic signal can be obtained by substituting the value of each parameter shown in Table 1 into Eq. (10), and Fig. 6 shows its time domain waveform and Hilbert envelope spectrum. From Fig. 6(a) it appears that the simulated impulse component is difficult to be recognized because of the interference of the simulated harmonic component and Gaussian white noise. As can be seen from Fig. 6(b), the amplitude at f_2-f_1 is quite big and prominent, but the amplitudes at f_c and its harmonics are too small to be detected. In short, the state of the rolling bearing cannot be directly determined according to the Hilbert envelope spectrum of the synthetic signal.

The synthetic signal is subjected to the WHVG-GFT method. At first, the synthetic signal is transformed into the WHVG whose

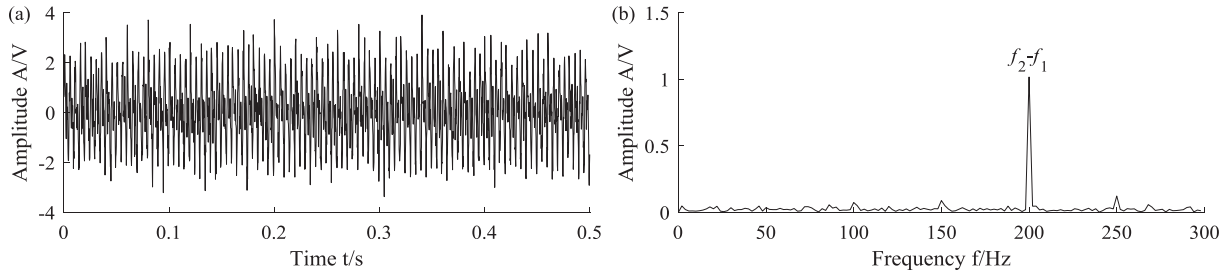

Fig. 6. Time domain waveform and Hilbert envelope spectrum of the synthetic signal. (a) Time domain waveform; (b) Hilbert envelope spectrum.

edge weight is defined by Eq. (2), and the synthetic signal is indexed by the WHVG to acquire the synthetic graph signal whose values correspond to the values of the synthetic signal one by one. Then the GFT of the synthetic graph signal is performed by Eq. (6) to obtain the corresponding graph spectrum. For comparative analysis, the FT of the synthetic signal is also calculated. Fig. 7(a) and (b) show its frequency spectrum and graph spectrum, respectively.

As shown in Fig. 7(a) and (b), there is a huge difference between the frequency spectrum and graph spectrum of the synthetic signal. In the frequency spectrum, the energy of the synthetic signal is basically concentrated at the frequencies f_1 and f_2. In the graph spectrum, although the energy of the synthetic signal is distributed over the entire order range, the graph spectrum coefficients in the vicinity of orders 200 and 400 and in the highest order range are more prominent. On the basis of the analysis results in the third section, we can infer that the graph spectrum coefficients in the highest order range should reveal the impulse characteristics of the synthetic signal.

Therefore, the last K coefficients are retained and the remaining coefficients are discarded in the graph spectrum to reconstruct the impulse component in the synthetic signal. The reconstructed impulse component is subjected to the Hilbert envelope demodulation analysis. When K is equal to 40, the time domain waveform and Hilbert envelope spectrum of the reconstructed impulse component are displayed in Fig. 8. From the comparison between Fig. 8 (a) and Fig. 2(a), we can see that the reconstructed impulse component is basically the same as the simulated impulse component except for the amplitude differences. Seen from Fig. 8(b), the amplitudes of f_c and its harmonics are very obvious. This means that the fault of the rolling bearing can be successfully diagnosed by the WHVG-GFT method.

For the sake of analyzing the effect of the unique parameter K on the WHVG-GFT method, only the value of the parameter K is changed from 40 to 30, 35, 45 or 50, and the other steps remain unchanged. Fig. 9 shows the Hilbert envelope spectrum of the reconstructed impulse component with K equaling to 30, 35, 45 or 50. From the comparison between Fig. 8(b) and Fig. 9, we can see that the contours of these Hilbert envelope spectra are basically the same, and the amplitudes of f_c and its harmonics are only slightly different. These indicate that the extraction result of the WHVG-GFT method is not sensitive to the value of the parameter K, and thus the value of the parameter K can be taken over a fairly wide range in the WHVG-GFT method. In order to facilitate the analysis, the value of the parameter K is taken as 40 for the WHVG-GFT method in the remainder of this paper.

Naturally, a nice impulse component extraction method should have strong anti-noise ability. In this study, noise with different SNR is added to the synthetic signal to compare the performances of the WHVG-GFT, WPG-GFT and spectral kurtosis methods. In order to ensure the comparability, the last 40 graph spectrum coefficients are retained and the remaining coefficients are discarded to reconstruct the impulse component for the WHVG-GFT and WPG-GFT methods. Figs. 10–12 show the Hilbert envelope spectra of the impulse components extracted by these three

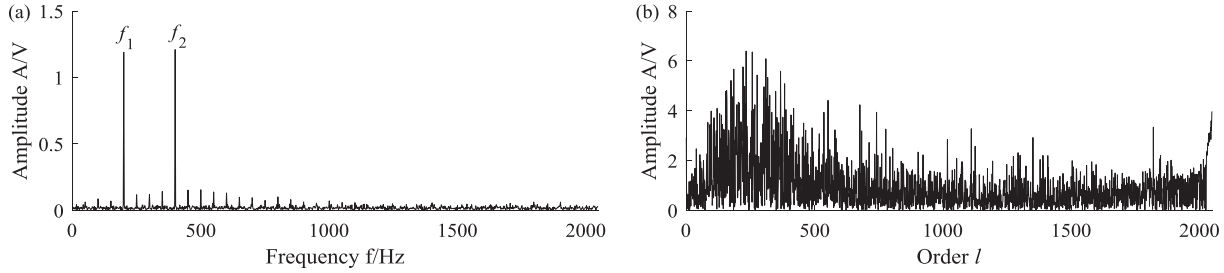

Fig. 7. Frequency spectrum and graph spectrum of the synthetic signal. (a) Frequency spectrum; (b) Graph spectrum.

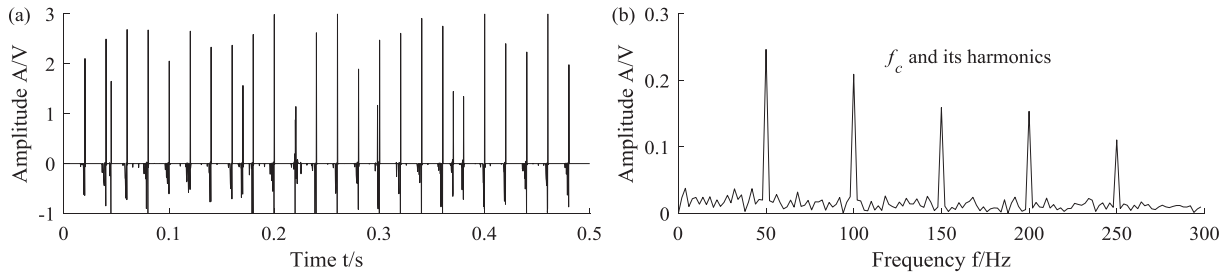

Fig. 8. Time domain waveform and Hilbert envelope spectrum of the reconstructed impulse component. (a) Time domain waveform; (b) Hilbert envelope spectrum.

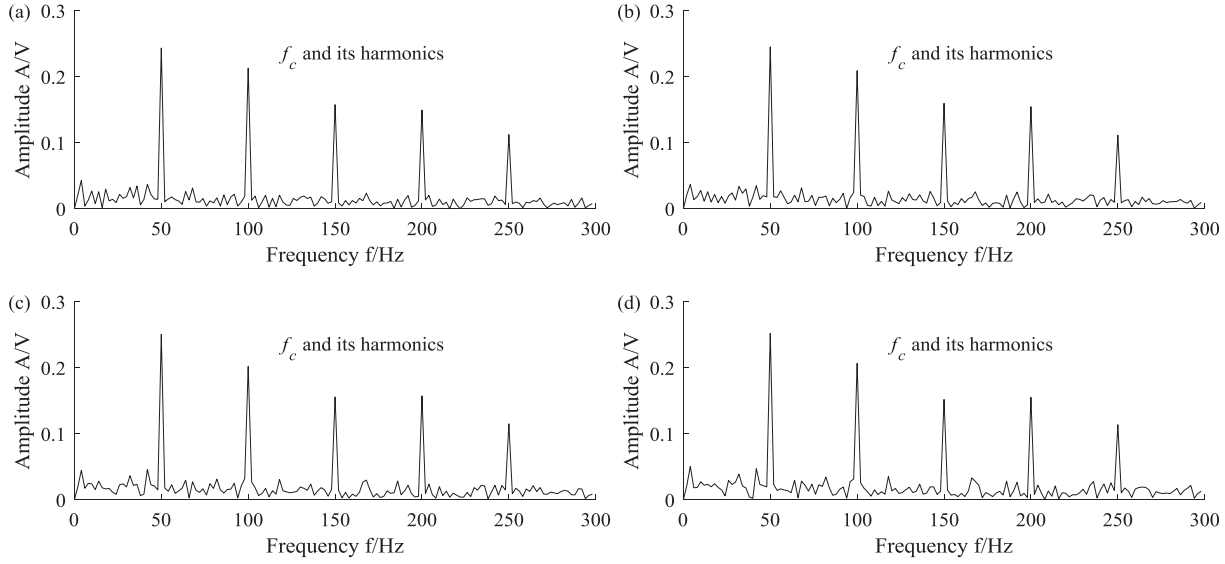

Fig. 9. Hilbert envelope spectrum of the reconstructed impulse component with different *K*. (a) *K* = 30; (b) *K* = 35; (c) *K* = 45; (d) *K* = 50.

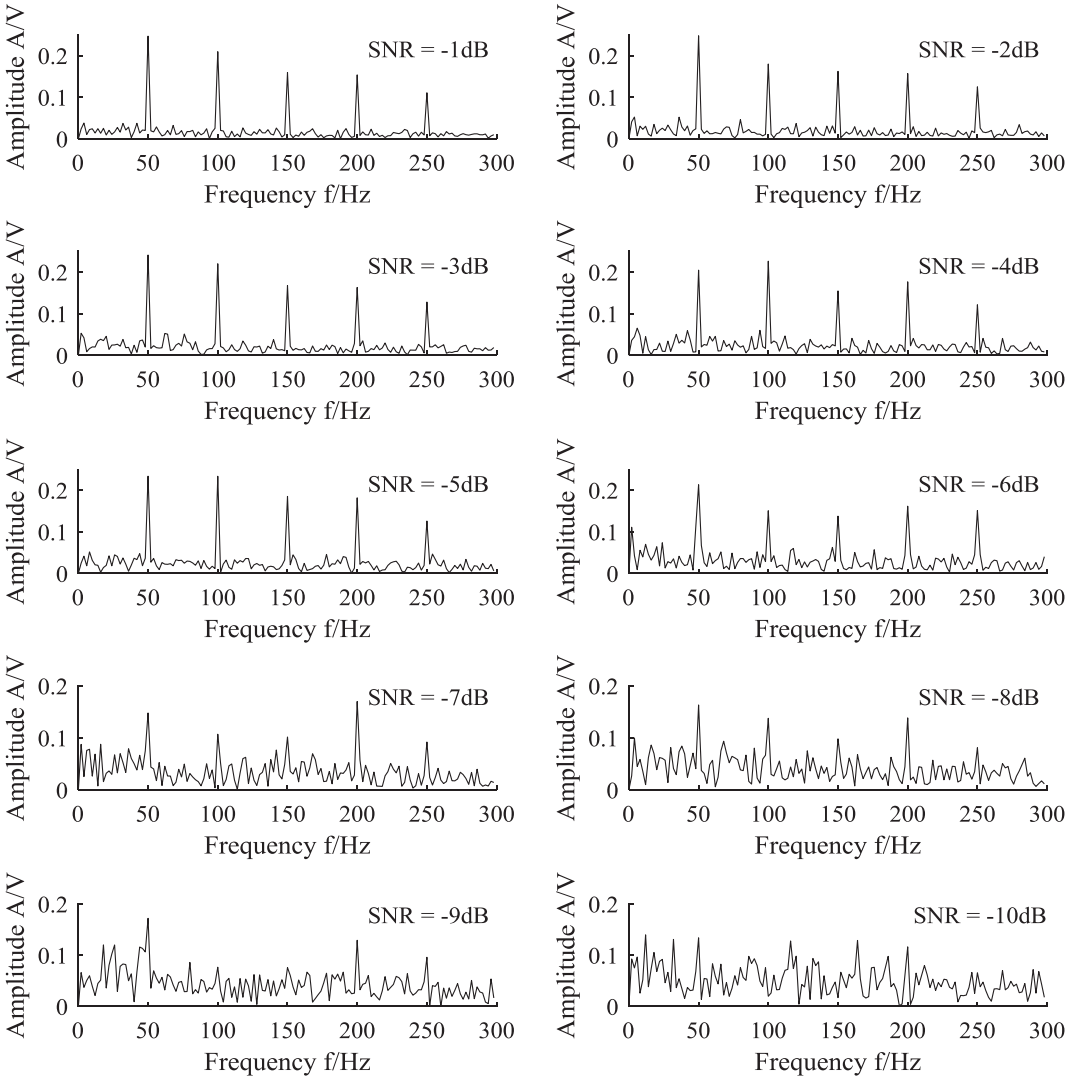

Fig. 10. Effect of noise on the WHVG-GFT method.

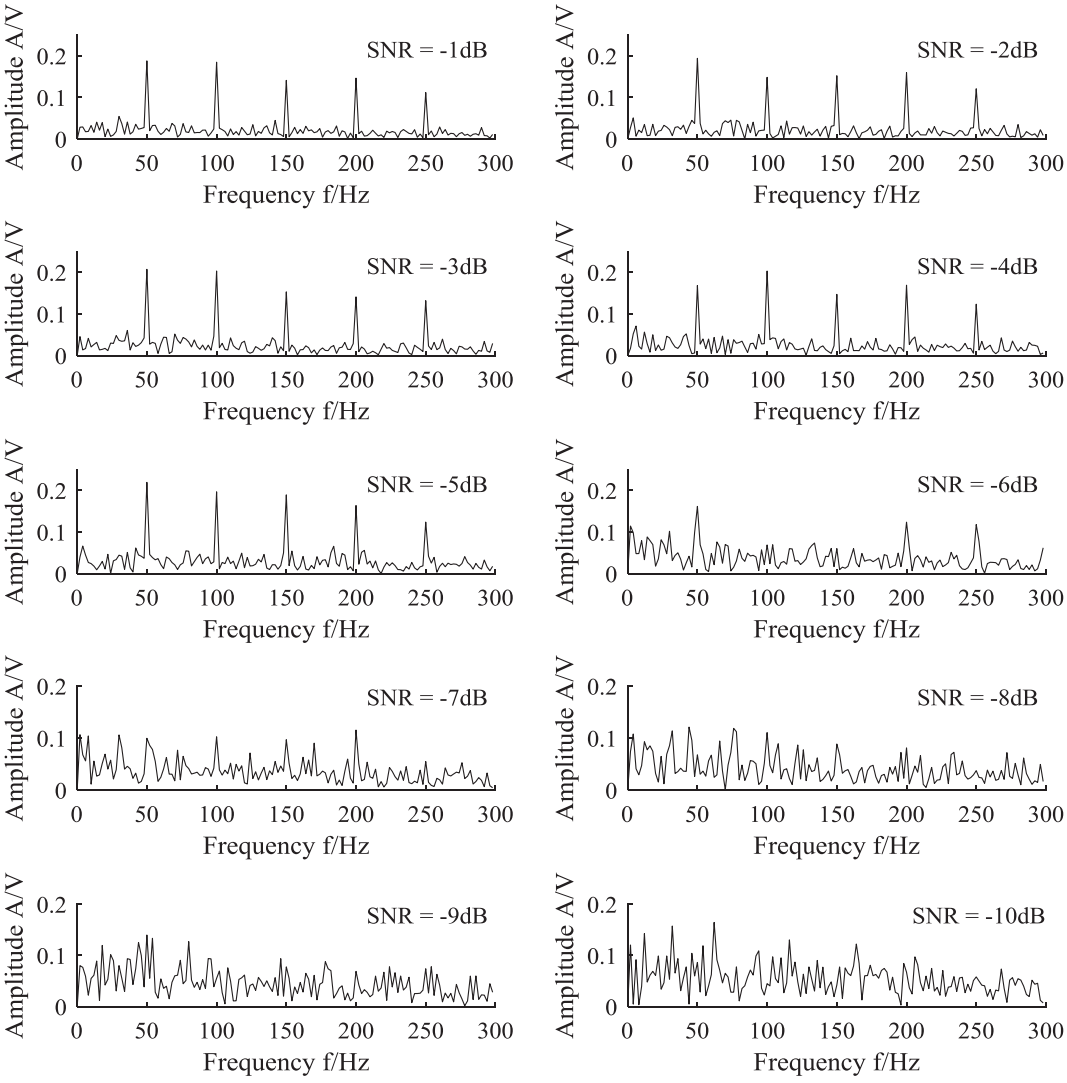

Fig. 11. Effect of noise on the WPG-GFT method.

methods, respectively. In Fig. 10, when the SNR is between −1dB and −9dB, f_c and its harmonics can be easily detected. In Fig. 11, only when the SNR is between −1dB and −6dB, f_c and its harmonics can be easily detected. In Fig. 12, only when the SNR is between −1dB and −5dB, f_c and its harmonics can be easily detected. Overall, it may be said that the WHVG-GFT method has stronger anti-noise ability than the WPG-GFT and spectral kurtosis methods.

6. Experimental validations

In order to verify the effectiveness of the WHVG-GFT method in rolling bearing fault diagnosis, two application examples for diagnosing the local fault in the outer ring and inner ring are given in this section. The test bench presented in Fig. 13 is composed of a driver motor, a coupling, a rotor and a shaft with two 6311-type roller bearings. A groove with the width of 0.15 mm and depth of 0.13 mm is made on the outer ring of rolling bearing to simulate the outer ring fault. Similarly, a groove with the width of 0.15 mm and depth of 0.13 mm is made on the inner ring of rolling bearing to simulate the inner ring fault. The vibration acceleration sensors were mounted on the pedestal of the faulty rolling bearing, and the vibration signals were collected by the LMS data sampling box at a sampling frequency of 4096 Hz. In the following two experimental signals, the sampling time is take as 0.25 s, so the number of sampling points is 1024.

6.1. Rolling bearing with an outer ring fault

The effectiveness of the WHVG-GFT method is again verified by diagnosing the outer ring fault of an actual rolling bearing. When the outer ring fault vibration signal was collected, the axis rotated at a speed of 1500 r/min, so the rotational frequency of the axis f_r is 25 Hz. The characteristic frequency of the outer ring fault f_o is equal to 76 Hz. Since it cannot be judged whether the outer ring fault vibration signal shown in Fig. 14(a) includes the fault impulse component, it needs to be analyzed and processed. The outer ring fault vibration signal is directly subjected to the Hilbert envelope demodulation analysis to obtain its Hilbert envelope spectrum. From Fig. 14(b), we can see that f_o is completely submerged by the interference frequencies next to it, which indicates that the outer ring fault cannot be directly diagnosed by the Hilbert envelope spectrum of the outer ring fault vibration signal.

The WHVG-GFT, WPG-GFT and spectral kurtosis methods are applied to process the outer ring fault vibration signal, respectively. For the WHVG-GFT and WPG-GFT methods, the last 40 graph spectrum coefficients are retained and the remaining coefficients are discarded to reconstruct the fault impulse component. Figs. 15–17 display the extraction results of these three methods, respectively. From Fig. 15(b), we can see that evidently peaks appear at f_o and $2f_o$, which suggests that the fault impulse component plotted in Fig. 15(a) is modulated by the characteristic

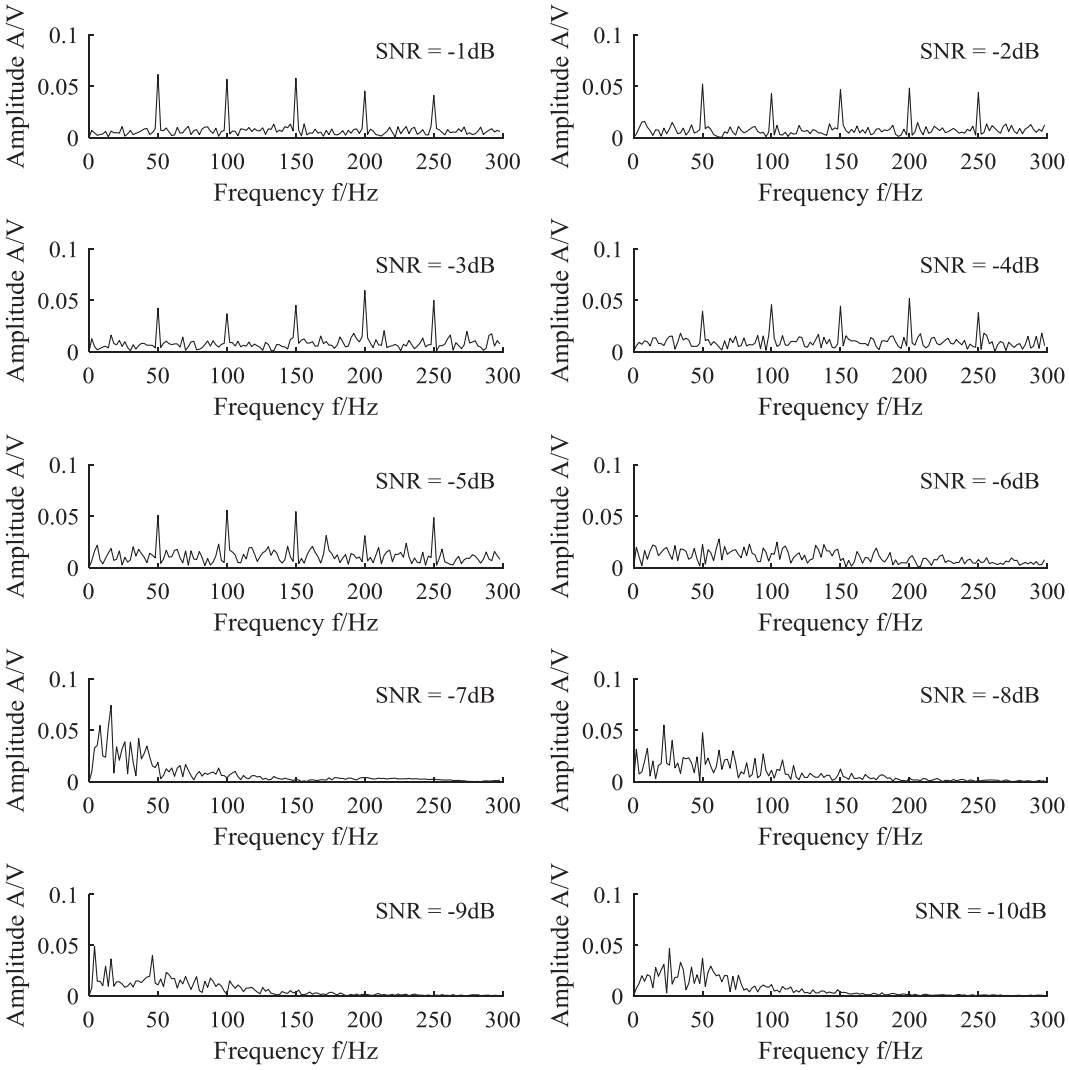

Fig. 12. Effect of noise on the spectral kurtosis method.

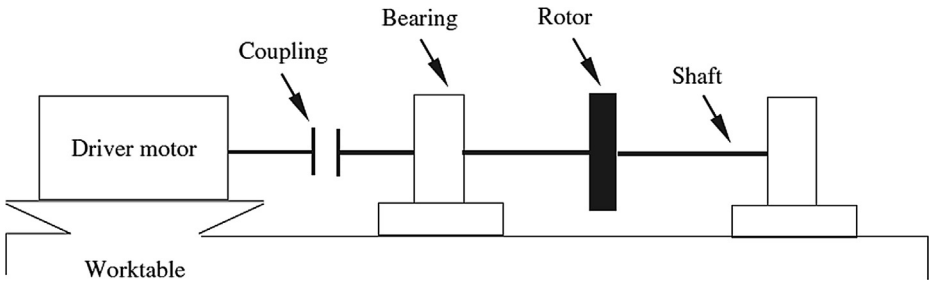

Fig. 13. The test bench.

frequency of the outer ring fault, and the outer ring fault is accurately diagnosed by the WHVG-GFT method. From Fig. 16(b), it can be observed that the interference frequency 84 Hz is more obvious than f_o. In Fig. 17(c), f_o cannot be recognized at all. In summary, the WHVG-GFT method is superior to the WPG-GFT and spectral kurtosis methods in diagnosing the outer ring fault in this experiment.

6.2. Rolling bearing with an inner ring fault

The effectiveness of the WHVG-GFT method is further validated by diagnosing the inner ring fault of an actual rolling bearing. When the inner ring fault vibration signal was collected, the axis rotated at a speed of 1200 r/min, so the rotational frequency of the axis f_r is 20 Hz. The characteristic frequency of the inner ring fault f_i is equal to 100 Hz. We can observe that the inner ring fault vibration signal shown in Fig. 18(a) contains many impulses, but the fault position of the rolling bearing cannot be determined. The inner ring fault vibration signal is directly subjected to the Hilbert envelope demodulation analysis to obtain its Hilbert envelope spectrum. In Fig. 18(b), although there are peaks at f_i and $2f_i$, the interference frequencies are more prominent. Consequently, the inner ring fault cannot be diagnosed by the Hilbert envelope spectrum of the inner ring fault vibration signal too.

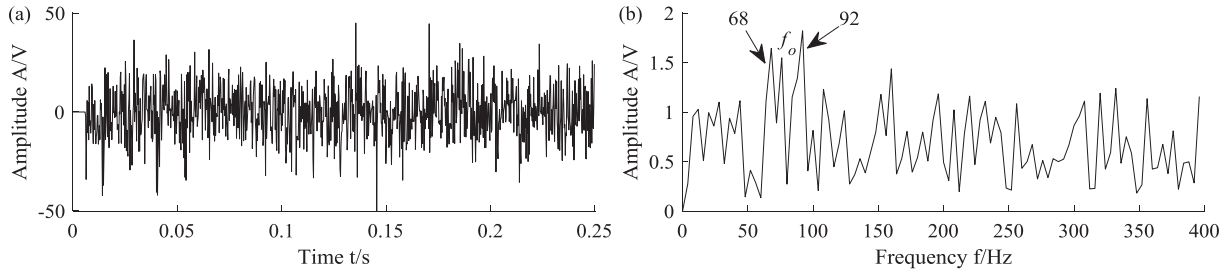

Fig. 14. Time domain waveform and Hilbert envelope spectrum of the outer ring fault vibration signal. (a) Time domain waveform; (b) Hilbert envelope spectrum.

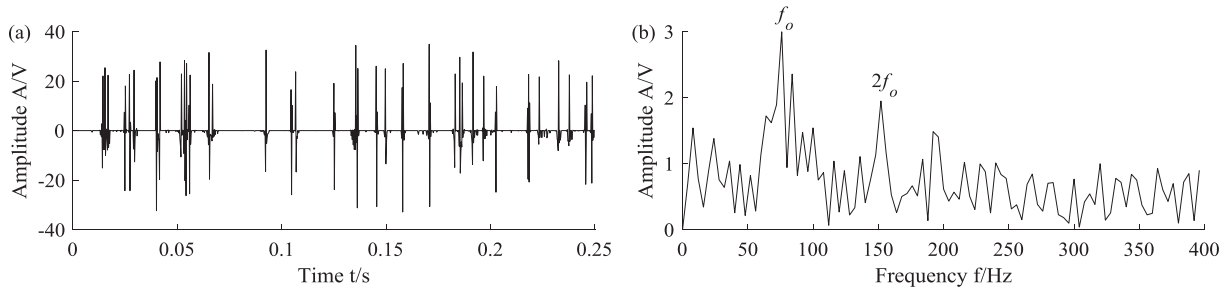

Fig. 15. Extraction result of the WHVG-GFT method for the outer ring fault vibration signal. (a) Time domain waveform; (b) Hilbert envelope spectrum.

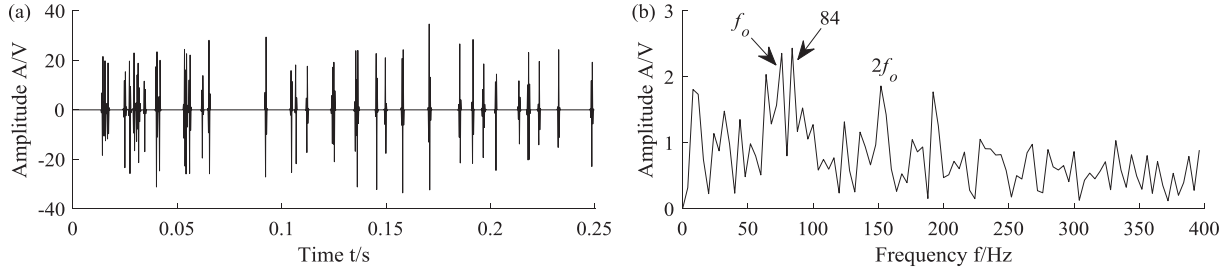

Fig. 16. Extraction result of the WPG-GFT method for the outer ring fault vibration signal. (a) Time domain waveform; (b) Hilbert envelope spectrum.

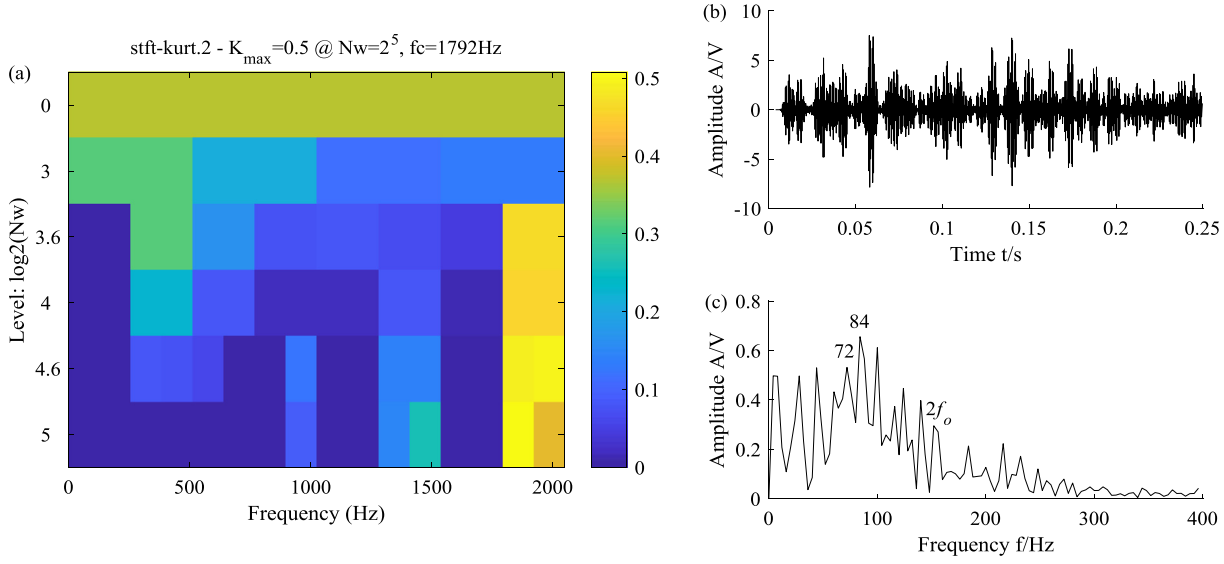

Fig. 17. Extraction result of the spectral kurtosis method for the outer ring fault vibration signal. (a) Kurtogram; (b) Time domain waveform; (c) Hilbert envelope spectrum.

The WHVG-GFT, WPG-GFT and spectral kurtosis methods are applied to process the inner ring fault vibration signal, respectively. For the WHVG-GFT and WPG-GFT methods, the last 40 graph spectrum coefficients are retained and the remaining coefficients are discarded to reconstruct the fault impulse component. Figs. 19–21 exhibit the extraction results of these three methods,

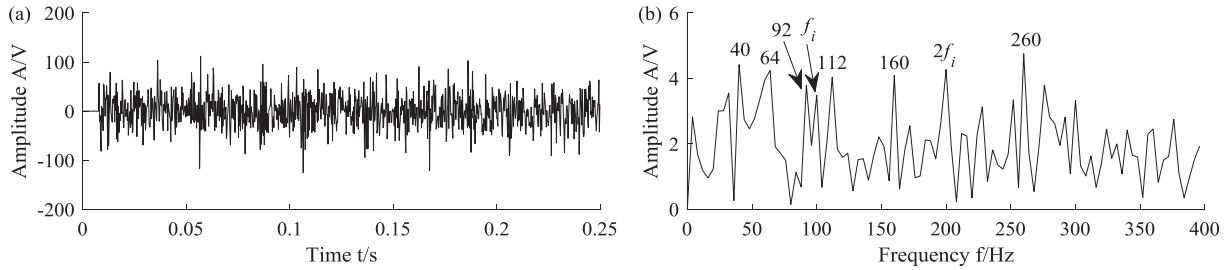

Fig. 18. Time domain waveform and Hilbert envelope spectrum of the inner ring fault vibration signal. (a) Time domain waveform; (b) Hilbert envelope spectrum.

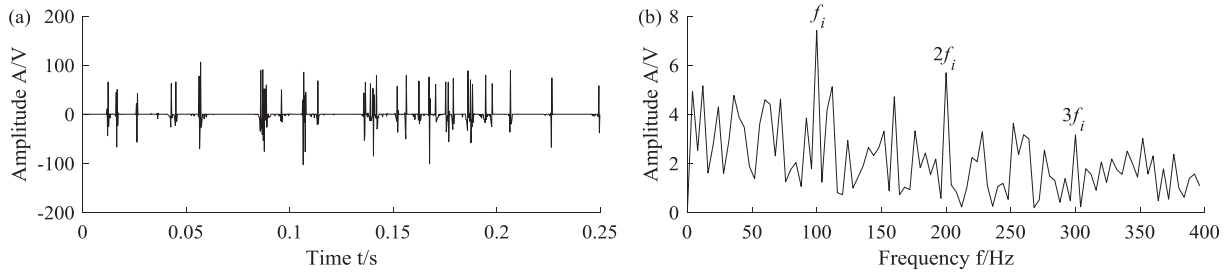

Fig. 19. Extraction result of the WHVG-GFT method for the inner ring fault vibration signal. (a) Time domain waveform; (b) Hilbert envelope spectrum.

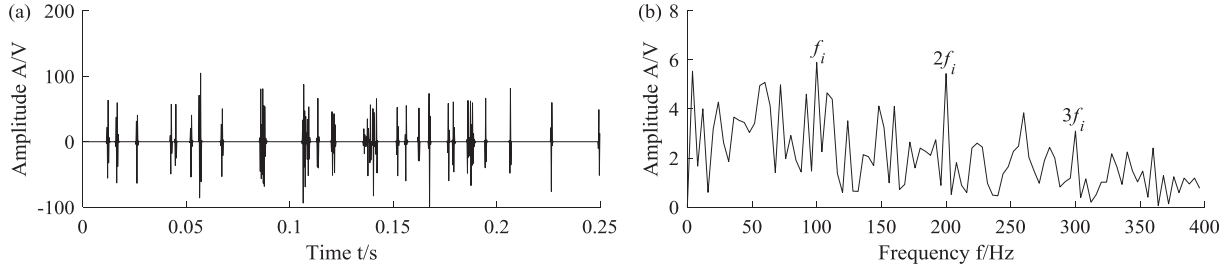

Fig. 20. Extraction result of the WPG-GFT method for the inner ring fault vibration signal. (a) Time domain waveform; (b) Hilbert envelope spectrum.

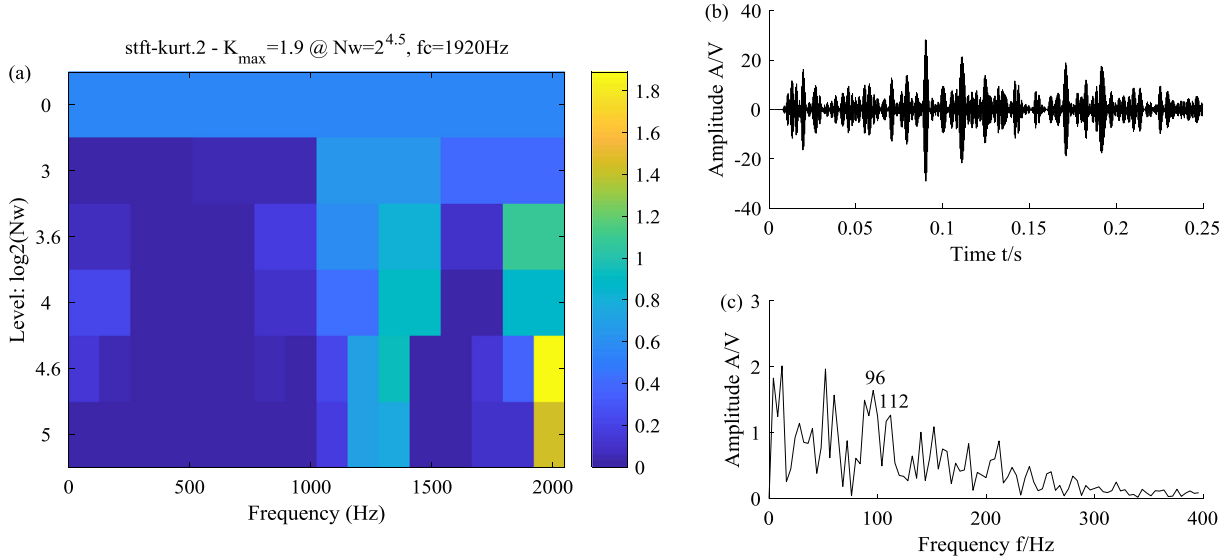

Fig. 21. Extraction result of the spectral kurtosis method for the inner ring fault vibration signal. (a) Kurtogram; (b) Time domain waveform; (c) Hilbert envelope spectrum.

respectively. In Fig. 19(b), we can observe that obvious peaks appear at f_i, $2f_i$ and $3f_i$, which means that the fault impulse component plotted in Fig. 19(a) is modulated by the characteristic frequency of the inner ring fault, and the inner ring fault is accurately diagnosed by the WHVG-GFT method. It is easy to see that f_i, $2f_i$ and $3f_i$ in Fig. 20(b) are not as prominent as those in Fig. 19(b). In Fig. 21(c), f_i, $2f_i$ and $3f_i$ cannot be recognized at all. To sum up, the WHVG-GFT method is better than the WPG-GFT and spectral kurtosis methods in diagnosing the inner ring fault in this experiment.

7. Conclusions

The key to fault diagnosis of rolling bearing is to extract the fault impulse component from its vibration signal. For better extracting the fault impulse component, the WHVG and GFT are simultaneously introduced to analyze the rolling bearing vibration signals. The impulse and harmonic components are the main components of the rolling bearing vibration signals, so the WHVG based GFT analysis of their simulated signals is first performed. As the impulse and harmonic components can be clustered to different order ranges, and the former is largely clustered to the highest order range, a novel impulse component extraction method for rolling bearing fault diagnosis using WHVG and GFT is presented in this study. Eventually, both the constructed simulation signal and the collected experiment signals are utilized to verify the effectiveness of the WHVG-GFT method. The main conclusions of this study are provided below.

(1) The horizontal visibility algorithm establishes a mapping between time series and horizontal visibility graphs. Since the mechanical vibration signal is a typical time series, it can also be transformed into a horizontal visibility graph by means of the horizontal visibility algorithm. The horizontal visibility graph can more fully reflect the dynamics characteristics of a mechanical vibration signal than the path graph.
(2) The GFT is defined as the expansion of graph signals based on the graph Laplacian eigenvectors in this study. The graph Laplacian eigenvectors play a key role in spectral clustering. After transforming the bearing vibration signal into the WHVG, the fault impulse component can be largely clustered to the highest order range and the harmonic component can be largely clustered to the relatively low order range by the GFT.
(3) The effectiveness and superiority of the proposed WHVG-GFT method for fault diagnosis of rolling bearings have been demonstrated by simulation and experimental signals. In particular, the WHVG-GFT method has strong robustness to the parameter K, which can be selected over a fairly wide range.

Declaration of Competing Interest

The authors declare that they have no known competing financial interests or personal relationships that could have appeared to influence the work reported in this paper.

Acknowledgment

This study was supported by the National Natural Science Foundation of China (Grant no. 51875182).

References

[1] L. Wang, Z. Liu, Q. Miao, et al., Complete ensemble local mean decomposition with adaptive noise and its application to fault diagnosis for rolling bearings, Mech. Syst. Sig. Process. 106 (2018) 24–39.
[2] L. Cui, J. Huang, F. Zhang, Quantitative and localization diagnosis of a defective ball bearing based on vertical-horizontal synchronization signal analysis, IEEE Trans. Ind. Electron. 64 (2017) 8695–8706.
[3] X. Zhang, Z. Liu, Q. Miao, et al., An optimized time varying filtering based empirical mode decomposition method with grey wolf optimizer for machinery fault diagnosis, J. Sound Vib. 418 (2018) 55–78.
[4] L. Cui, Y. Zhang, F. Zhang, et al., Vibration response mechanism of faulty outer race rolling element bearings for quantitative analysis, J. Sound Vib. 364 (2016) 67–76.
[5] X.Q. Xu, J. Lin, C. Yan, Adaptive determination of fundamental frequency for direct time-domain averaging, Measurement 124 (2018) 351–358.
[6] Z.K. Peng, F.L. Chu, Application of the wavelet transform in machine condition monitoring and fault diagnostics: a review with bibliography, Mech. Syst. Sig. Process. 18 (2004) 199–221.
[7] H.R. Cao, F. Fan, K. Zhou, et al., Wheel-bearing fault diagnosis of trains using empirical wavelet transform, Measurement 82 (2016) 439–449.
[8] J. Antoni, R.B. Randall, The spectral kurtosis: application to the vibratory surveillance and diagnostics of rotating machines, Mech. Syst. Sig. Process. 20 (2006) 308–331.
[9] L. Cui, J. Wang, S. Lee, Matching pursuit of an adaptive impulse dictionary for bearing fault diagnosis, J. Sound Vib. 333 (2014) 2840–2862.
[10] Y. Lei, J. Lin, Z. He, et al., A review on empirical mode decomposition in fault diagnosis of rotating machinery, Mech. Syst. Sig. Process. 35 (2013) 108–126.
[11] H.M. Zhao, M. Sun, W. Deng, et al., A new feature extraction method based on EEMD and multi-scale fuzzy entropy for motor bearing, Entropy 19 (1) (2017) 14.
[12] W. Deng, J.J. Xu, H.M. Zhao, An improved ant colony optimization algorithm based on hybrid strategies for scheduling problem, IEEE Access 7 (2019) 20281–20292.
[13] W. Deng, H.M. Zhao, L. Zou, et al., A novel collaborative optimization algorithm in solving complex optimization problems, Soft Comput. 21 (2017) 4387–4398.
[14] H.M. Zhao, R. Yao, L. Xu, et al., Study on a novel fault damage degree identification method using high-order differential mathematical morphology gradient spectrum entropy, Entropy 20 (2018) 18.
[15] J. Antoni, The spectral kurtosis: a useful tool for characterising non-stationary signals, Mech. Syst. Sig. Process. 20 (2006) 282–307.
[16] Y.X. Wang, J.W. Xiang, R. Markert, et al., Spectral kurtosis for fault detection, diagnosis and prognostics of rotating machines: a review with applications, Mech. Syst. Sig. Process. 66–67 (2016) 679–698.
[17] D.I. Shuman, S.K. Narang, P. Frossard, et al., The emerging field of signal processing on graphs: extending high-dimensional data analysis to networks and other irregular domains, Signal Proc. Magn. 30 (2013) 83–98.
[18] A. Sandryhaila, J.M.F. Moura, Discrete signal processing on graphs, Trans. Signal Process. 61 (2013) 1644–1656.
[19] A. Sandryhaila, J.M.F. Moura, Discrete signal processing on graphs: frequency analysis, Trans. Signal Process. 62 (2014) 3042–3054.
[20] D.I. Shuman, B. Ricaud, P. Vandergheynst, Vertex-frequency analysis on graphs, Appl. Comput. Harmon. A. 40 (2013) 260–291.
[21] D.K. Hammond, P. Vandergheynst, R. Gribonval, Wavelets on graphs via spectral graph theory, Appl. Comput. Harmon. A. 30 (2009) 129–150.
[22] D.I. Shuman, C. Wiesmeyr, N. Holighaus, et al., Spectrum-adapted tight graph wavelet and vertex-frequency frames, Trans. Sig. Process. 63 (2015) 4223–4235.
[23] N. Tremblay, P. Borgnat, P. Flandrin, Graph empirical mode decomposition, in: Signal Processing Conference (EUSIPCO), 2014 Proceedings of the 22nd European, IEEE, 2014, pp. 2350–2354.
[24] A. Venkitaraman, S. Chatterjee, P. Händel, Hilbert transform, analytic signal, and modulation analysis for graph signal processing, 2016.
[25] A. Sandryhaila, J.M.F. Moura, Big data analysis with signal processing on graphs: representation and processing of massive data sets with irregular structure, Signal Proc. Magn. 31 (2014) 80–90.
[26] S. Chen, F. Cerda, P. Rizzo, et al., Semi-supervised multiresolution classification using adaptive graph filtering with application to indirect bridge structural health monitoring, Trans. Signal Process. 62 (2014) 2879–2893.
[27] L. Ou, D.J. Yu, H.J. Yang, A new rolling bearing fault diagnosis method based on GFT impulse component extraction, Mech. Syst. Sig. Process. 81 (2016) 162–182.
[28] L. Ou, D.J. Yu, Compound fault diagnosis of gearboxes based on GFT component extraction, Meas. Sci. Technol. 27 (2016) 115007.
[29] L. Ou, D.J. Yu, Fault diagnosis of roller bearings based on Laplacian energy feature extraction of path graphs, Measurement 91 (2016) 168–176.
[30] B. Luque, L. Lacasa, F. Ballesteros, et al., Horizontal visibility graphs: exact results for random time series, Phys. Rev. E 80 (2009).
[31] U.V. Luxburg, A tutorial on spectral clustering, Stat. Comput. 17 (2007) 395–416.
[32] M. Liang, I.S. Bozchalooi, An energy operator approach to joint application of amplitude and frequency-demodulations for bearing fault detection, Mech. Syst. Sig. Process. 24 (2010) 1473–1494.